Impact of Threading Dislocations on the Design of GaAs and InGaP/GaAs Solar Cells on Si Using Finite Element Analysis

Nikhil Jain, *Student Member, IEEE*, and Mantu K. Hudait, *Senior Member, IEEE*

***Abstract*—We investigate the impact of threading dislocation densities on the photovoltaic performance of single-junction (1J) n^+/p GaAs and dual-junction (2J) n^+/p InGaP/GaAs solar cells on Si substrate. Using our calibrated model, simulation predicts an efficiency of greater than 23% for a 1J GaAs cell on Si at AM1.5G spectrum at a threading dislocation density of 10^6 cm^{-2}. The design of a metamorphic 2J InGaP/GaAs solar cell on Si was optimized by tailoring the 2J cell structure on Si to achieve current matching between the subcells, taking into account a threading dislocation density of 10^6 cm^{-2}. Finally, we present a novel and an optimized 2J InGaP/GaAs solar cell design on Si at a threading dislocation density of 10^6 cm^{-2}, which exhibited a theoretical conversion efficiency of greater than 29% at AM1.5G spectrum, indicating a path for viable III–V multijunction cell technology on Si.**

***Index Terms*—III–V semiconductor materials, charge carrier lifetime, photovoltaic cells, semiconductor device modeling.**

I. Introduction

MULTIJUNCTION III–V solar cells are the dominant choice for space satellite power, primarily due to their high efficiencies under concentrated sunlight [1]–[4]. Efficiencies as high as 43.5% have been demonstrated for GaInP/GaAs/GaInNAs III–V solar cells under 418x suns [5]. However, the higher costs of Ge and III–V substrates have restricted the widespread commercialization of III–V solar cells. Heteroepitaxy of III–V materials on large diameter, cheaper, and readily available Si substrate will not only offer a path for low cost and high-efficiency III–V cells but also significantly increase their yield per die. Furthermore, the implementation of III–V solar cells on Si in conjunction with substrate reuse technologies [6], [7] can lead to additional cost savings. However, viability of III–V InGaP/GaAs solar cells on Si relies on the ability to grow high-quality GaAs on Si with careful lattice engineering and substrate treatment. The polar-on-nonpolar epitaxy and the 4% lattice mismatch between GaAs and Si may result in the formation of various defects including dislocations. These dislocations can propagate into the photoactive cell region, significantly impeding the minority carrier lifetime and, hence, the overall cell performance [8]–[11].

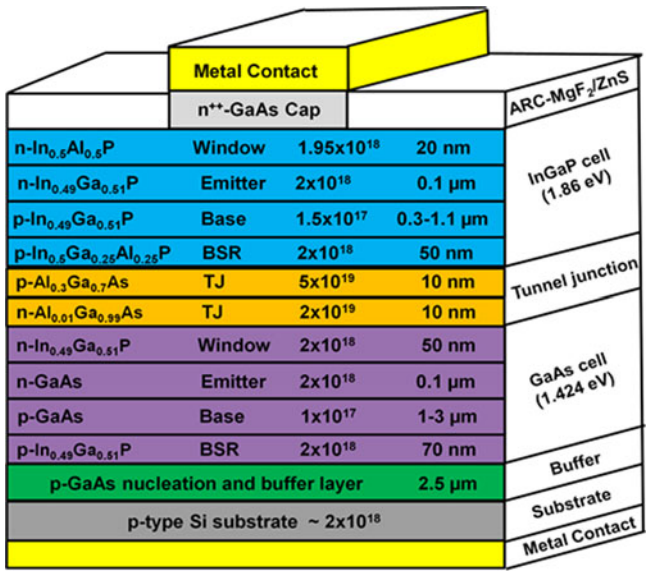

Fig. 1. Schematic depiction of a 2J InGaP/GaAs solar cell on Si.

The focus of this paper is to provide a systematic study on the correlation of threading dislocation density (TDD) and minority carrier lifetime on the single-junction (1J) and dual-junction (2J) cell figure of merits, namely, efficiency η, open-circuit voltage $V_{\rm oc}$, short-circuit current density $J_{\rm sc}$, and fill factor (FF). The schematic of the 2J InGaP/GaAs cell structure investigated in this paper is shown in Fig. 1. As a starting point in our simulation, the base thicknesses in the GaAs and InGaP cell were set to be 2.5 and 0.9 μm, respectively [1]. We then discuss our design methodology to engineer the metamorphic 2J InGaP/GaAs cell structure on Si to achieve the current-matching condition between the subcells at a TDD of 10^6 cm^{-2}. The results from our detailed cell modeling provide a quantitative assessment of solar cell figures of merit as a function of TDD, thus enabling more efficient cell design and prediction of the metamorphic 2J cell performance on Si.

The impact of TDD on cell performance has been previously investigated [9]–[14]; however, their analysis was limited to only 1J GaAs cell on Si. For modeling the impact of TDD on $V_{\rm oc}$, $J_{\rm sc}$ was assumed to be independent of TDD [13]. In reality, $J_{\rm sc}$ decreases with an increase in TDD and may have a significant impact on the extraction of efficiency. Recently, the

Manuscript received February 13, 2012; accepted July 31, 2012. Date of publication September 4, 2012; date of current version December 19, 2012. This work was supported in part by the Institute for Critical Technology and Applied Sciences, Virginia Tech, Blacksburg.

The authors are with the Advanced Devices and Sustainable Energy Laboratory, Bradley Department of Electrical and Computer Engineering, Virginia Tech, Blacksburg, VA 24061 USA (e-mail: jain34@vt.edu; mantu@vt.edu).

Color versions of one or more of the figures in this paper are available online at http://ieeexplore.ieee.org.

Digital Object Identifier 10.1109/JPHOTOV.2012.2213073

TABLE I
GaAs AND InGaP MATERIAL AND TRANSPORT PARAMETERS

Parameters (Abbreviation, Units)	GaAs	InGaP
Band-gap (E_g, eV)	1.424	1.86
Minority electron mobility (μ_e, cm^2/Vs)	3088.8	1074 [20]
Minority hole mobility (μ_h, cm^2/Vs)	100 [17]	40 [20]
Electron diffusion coefficient (D_n, cm^2/s)	80 [18]	27.816
Hole diffusion coefficient (D_p, cm^2/s)	2.59	1.036
Peak minority electron lifetime ($\tau°_n$, ns)	20 [12], [19]	10 [21], [22]
Minority hole lifetime ($\tau°_p$, ns)	2.5	1

impact of minority carrier lifetime on cell performance has been investigated for InGaN cells on Si [15]. The effect of dislocations in metamorphic III–V tandem cells has also been investigated but without incorporation of a substrate [16]. There has not been significant work done on the modeling-assisted design of metamorphic tandem solar cells incorporating the impact of TDD. This paper provides the first study on the modeling and the optimization of metamorphic 2J n^+/p InGaP/GaAs solar cell on Si at AM1.5G spectrum using finite element analysis without assuming a constant J_{sc}.

II. Simulation Model

Minority carrier lifetime is one of the most important figure of merit for the design of metamorphic solar cells. Defects and dislocations generated at the III–V/Si heterointerface may serve as recombination centers and decrease the minority carrier lifetime and, hence, their diffusion length. The effective minority carrier lifetime (τ_n or τ_p) in a lattice-mismatched system varies as a function of TDD ($f(\tau_{TDD})$) [12], [24] and is expressed as

$$\frac{1}{\tau_{n,p}} = \frac{1}{\tau^0_{n,p}} + \frac{1}{\tau_{TDD}} \tag{1}$$

where τ^0_p and τ^0_n are the minority carrier lifetime for a dislocation free material. The τ_{TDD} is the minority carrier lifetime associated with the recombination at dislocation and can be expressed as

$$\tau_{TDD} = \frac{4}{\pi^3 (TDD) D} \tag{2}$$

where D is the minority carrier diffusion coefficient, and TDD is the threading dislocation density in cm^{-2}.

Using the model described previously, coupled with the material parameters summarized in Table I, we computed the impact of TDD on the minority electron lifetime in p-GaAs and p-InGaP base, as shown in Fig. 2. Impact of TDD on minority carrier lifetime has been previously investigated in GaAs material [13]. From Fig. 2, it can be noted that for TDDs greater than 10^4 cm^{-2} in GaAs subcell, the minority electron lifetime significantly degraded. The onset of degradation in minority electron lifetime occurs at a higher TDD (10^5 cm^{-2}) in InGaP subcell compared with GaAs subcell due to the lower electron diffusion coefficient in p-InGaP material. By utilizing the minority electron lifetime variation as a function of increasing TDD, coupled with the material parameters incorporated from Table I, we simulated the impact of TDD on the performance of 1J GaAs and 2J InGaP/GaAs solar cells on Si [23]. The experimental lifetime values for p-GaAs (red) and p-InGaP (green) are included in this figure [19], [25], indicating an excellent agreement between the model and the experiment.

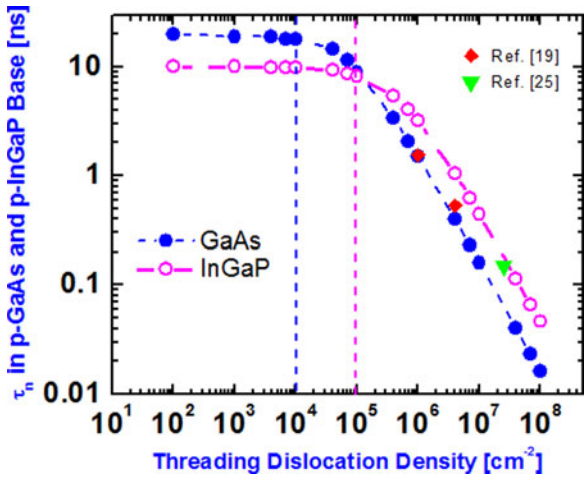

Fig. 2. Correlation of TDD on minority electron lifetime in p-GaAs and p-InGaP base.

In a solar cell, most of the light is absorbed in the thick base and the minority carriers generated far away from the junction should have sufficient lifetime to reach the junction before being recombined. Therefore, the variation of the minority electron lifetime in the base τ_n was found to have a significant impact on the cell performance. The minority hole lifetime τ_p in the thin emitter was considered to be constant. The surface recombination velocity (SRV) was set to 10^4 cm/s for both holes S_p and electrons S_n at InGaP base/back reflector interface and emitter/window interface. The corresponding S_n and S_p values were set to 10^6 cm/s at both the interfaces in the GaAs subcell. In our model, the mobility of minority carriers was assumed to be independent of TDD [24], and the effect of bandgap narrowing and grid shadowing was not included. Therefore, the analysis discussed in this paper provides an upper bound for the modeled cell results.

We calibrated our model with the 2J InGaP/GaAs cell structure in [26] and [27]. A τ_n value of 5.2 ns in p-InGaP was reported in [26]. This value of lifetime corresponds to a TDD of 4×10^5 cm^{-2}, as shown in Fig. 2. Since the value of τ_n in p-GaAs was not provided, a τ_n value of 3.3 ns was used from Fig. 2. The simulation results are compared with the experimental results in Table II. Overall, the simulated and the experimental values presented in Table II are in agreement, thus validating our model and the parameters utilized in the simulation.

III. Results and Discussion

This section is divided into four subsections. In Sections III-A and B, the impact of minority carrier lifetime degradation on the performance of 1J GaAs cell on Si and 2J InGaP/GaAs cell on

TABLE II
MODEL CALIBRATION WITH 2J InGaP/GaAs EXPERIMENTAL DATA

	V_{oc} (V)	J_{sc} (mA/cm^2)	FF (%)	Efficiency (%)
Experiment [26]	2.48	14.22	85.6	30.28
Simulation	2.41	13.85	88.9	29.80
Experiment [27]	2.52	12.70	85.00	27.20
Simulation	2.58	12.53	85.19	27.64

Si is discussed, respectively. Section III-C describes our design methodology to engineer the 2J InGaP/GaAs cell structure on Si to realize current matching between each subcell at a TDD of 10^6 cm^{-2}. Finally, Section III-D will discuss the impact of surface recombination on the 2J cell performance.

A. 1J GaAs Cell on Si

The p-GaAs base thickness in the 1J n$^+$/p GaAs cell on Si was set to 2.5 μm. The TDD in this GaAs cell was varied from 10^4 to 10^8 cm^{-2}. At a TDD of 10^6 cm^{-2}, the minority electron lifetime in p-GaAs was calculated to be 1.49 ns, as shown in Fig. 2, consistent with the experimentally determined minority electron lifetime of 1.5 ns in p-GaAs [19].

Voltages at maximum power point V_m and V_{oc} were plotted as a function of increasing TDD in the 1J GaAs cell on Si, as shown in Fig. 3(a). At lower TDD, the higher value of both V_{oc} and V_m was attributed to the higher minority electron lifetime in the p-GaAs base. TDD below 10^5 cm^{-2} had a negligible impact on the V_{oc}. However, beyond this TDD, V_{oc} started to degrade significantly. V_{oc} has a logarithmic dependence on reverse saturation current density J_0, which is inversely proportional to the minority carrier lifetime. Thus, at higher TDD, significant degradation in both V_{oc} and V_m was attributed to the higher reverse saturation current density pertaining to the reduced minority electron lifetime.

Current densities at maximum power point J_m and J_{sc} were plotted as a function of TDD in the 1J GaAs cell on Si, as shown in Fig. 3(b). For a TDD below 4×10^5 cm^{-2}, the minority electrons had sufficient lifetime to reach the junction before being recombined, and hence, TDD below 4×10^5 cm^{-2} had a negligible impact on the J_{sc}. For the 1J GaAs cell considered here, a τ_n value of at least 0.78 ns (at a TDD of 2×10^6 cm^{-2}) was necessary for the cell to function as a short diode. Beyond a TDD of 2×10^6 cm^{-2}, the cell behaved like a long diode with the electron diffusion length becoming shorter than the GaAs base thickness. Thus, beyond a TDD of 2×10^6 cm^{-2}, the degradation in both J_{sc} and J_m was attributed to the reduction in minority electron lifetime. Interestingly, from Fig. 3(a) and (b), it can be seen that the beginning of degradation in J_{sc} occurred at a higher TDD than V_{oc}, indicating that J_{sc} is more tolerant to TDD in the 1J GaAs cell on Si.

Fig. 3(c) shows the degradation in efficiency of the 1J GaAs cell on Si as a function of increasing TDD. It can be seen that cell efficiency higher than 25% was attained for TDD below 2×10^5 cm^{-2} (or τ_n greater than 5 ns). However, the cell effi-

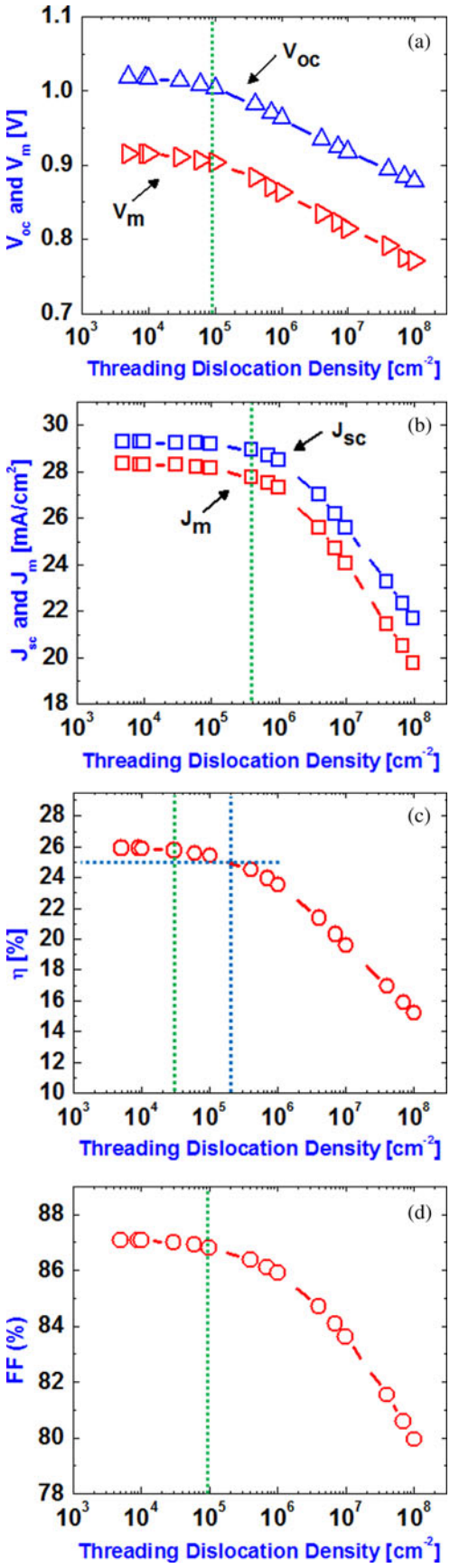

Fig. 3. Impact of TDD variation on 1J GaAs cell performance parameters. (a) V_{oc} and V_m, (b) J_{sc} and J_m, (c) η, and (d) FF at AM1.5G spectrum.

ciency significantly degraded beyond a TDD of $\sim 10^5$ cm^{-2} due to the reduction in both J_m and V_m, as discussed earlier. At an experimentally realistic TDD of 10^6 cm^{-2} [28], the corresponding cell efficiency was found to be 23.54%, while at a higher TDD of 10^7 cm^{-2}, the corresponding cell efficiency degraded to 19.61% due to the reduction in the minority electron lifetime.

The FF as a function of an increase in TDD was plotted in Fig. 3(d). There was almost negligible drop in the FF below a TDD of 10^5 cm^{-2}. The percentage drop in both J_m and V_m from a TDD of 10^4–10^8 cm^{-2} was greater than the percentage drop in $J_{\rm sc}$ and V_{oc}, respectively, as can be seen from Fig. 3(a) and (b). Thus, at higher TDD, a greater percentage drop in the $J_m \times V_m$ product compared with $J_{\rm sc} \times V_{\rm oc}$ led to the degradation in the FF.

B. 2J InGaP/GaAs Cell on Si

For the analysis of metamorphic 2J n$^+$/p InGaP/GaAs cell on Si, the base thicknesses in the GaAs and InGaP subcells were set to 2.5 and 0.9 μm, respectively. The TDD was varied from 10^5 to 10^8 cm^{-2}, and it was assumed that all the threading dislocations in GaAs bottom subcell propagated to the top InGaP subcell.

Fig. 4(a) shows the degradation in both $V_{\rm oc}$ and V_m as a function of increasing TDD in the 2J InGaP/GaAs cell on Si. The primary reason for the decrease in $V_{\rm oc}$ was due to the strong dependence on the reverse saturation current density J_{02} associated with the depletion region recombination. The $V_{\rm oc}$ can be expressed as

$$V_{\rm oc} = \left(\frac{n_2 kT}{q}\right) \ln\left(\frac{J_{\rm sc}}{J_{02}}\right) \tag{3}$$

where J_{02} depends on the minority carrier base lifetime $\tau_{\rm base}$ and is expressed as

$$J_{02} = \frac{q n_i W_D}{2}\left(\frac{1}{\tau_{\rm base}}\right) \tag{4}$$

where n_i is the intrinsic carrier concentration, and W_D is the depletion layer width. At higher TDD, the value of J_{02} increased due to the reduction in minority electron lifetime. Thus, the increase in J_{02} led to significant degradation in both $V_{\rm oc}$ and V_m with increasing TDD.

The $J_{\rm sc}$ and J_m in the 2J InGaP/GaAs cell were plotted as a function of an increase in TDD in Fig. 4(b). The degradation in both $J_{\rm sc}$ and J_m at higher TDD was due to the simultaneous reduction in the minority electron lifetime in both GaAs and InGaP base. The onset of degradation in $J_{\rm sc}$ in 2J cell configuration was also found to occur at higher TDD compared with $V_{\rm oc}$, similar to the 1J GaAs cell, which was discussed earlier. Thus, $J_{\rm sc}$ was more tolerant to TDD compared with $V_{\rm oc}$ for both 1J GaAs and 2J InGaP/GaAs cells on Si, which is consistent with prior work [14].

Fig. 4(c) shows the degradation of 2J InGaP/GaAs cell efficiency as a function of increasing TDD. At a TDD of 10^6 cm^{-2} in the 2J structure, the corresponding 2J cell efficiency was 26.22%. Beyond a TDD of 10^6 cm^{-2}, the degradation in minority electron lifetime in the p-GaAs significantly hindered the 2J InGaP/GaAs cell efficiency as p-GaAs material was found to

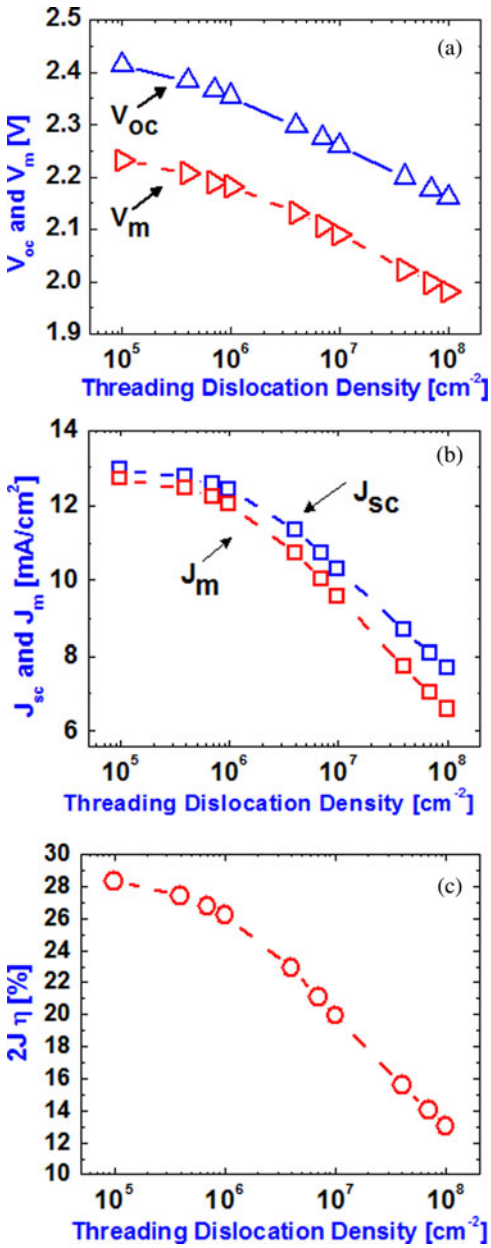

Fig. 4. Impact of TDD variation on 2J InGaP/GaAs cell performance parameters. (a) $V_{\rm oc}$ and V_m, (b) $J_{\rm sc}$ and J_m, and (c) η at AM1.5G spectrum.

be more sensitive to dislocations than the p-InGaP (see Fig. 2). Above a TDD of 10^7 cm^{-2}, the 2J InGaP/GaAs cell efficiency degraded to that of 1J GaAs cell efficiency, thus making the contribution of the top InGaP cell redundant.

The J–V characteristics of the 2J InGaP/GaAs (red curve) cell, the GaAs subcell (blue curve), and the InGaP subcell (pink curve) were plotted in Fig. 5 at a TDD of 10^6 cm^{-2}. It can be seen that the subcells were not current-matched and the bottom GaAs subcell limited the $J_{\rm sc}$ in the 2J cell configuration. In practice, it is challenging to improve the material quality of heteroepitaxial GaAs grown on Si to lower the TDD significantly below 10^6 cm^{-2}. Consequently, it becomes extremely important to optimize the metamorphic 2J InGaP/GaAs cell structure on

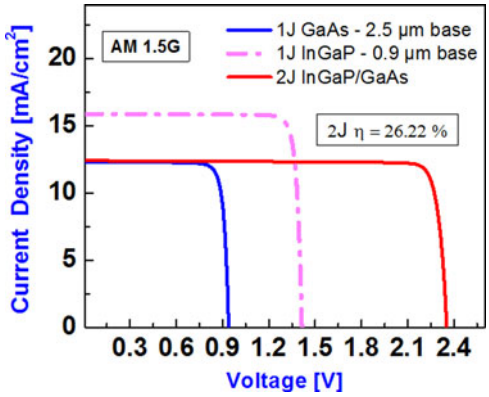

Fig. 5. J–V characteristic of a 2J cell along with the InGaP and GaAs subcells before current matching at a TDD of 10^6 cm^{-2} at AM 1.5G.

Si at a realistic TDD of 10^6 cm^{-2} by tailoring the design of each subcell.

C. Current Matching in 2J InGaP/GaAs Cell on Si

In a multijunction cell, one of the most important design criteria is to achieve the current matching between the subcells. Current matching enables us to extract the best performance from a multijunction cell. The cell with a higher bandgap provides a higher $V_{\rm oc}$ and a lower $J_{\rm sc}$. For achieving the current-matching condition, ideally, J_m between each subcell should be matched. Here, we used $J_{\rm sc}$ for current matching as $J_{\rm sc}$ is a directly measurable parameter during cell characterization, and it has been widely used for current-matching analysis [2], [29].

The subcells in our 2J configuration were not current-matched, as shown in Fig. 5. Therefore, appropriate design changes in our 2J cell structure were required to realize the current-matching condition between the subcells. In a solar cell, most of the light is absorbed in the thicker base layer, and hence, the minority carrier lifetime in the base plays a critical role in determining the current density contribution from a cell. Thus, we optimized the base thicknesses in the GaAs and the InGaP subcells to achieve current-matching condition at an experimentally realistic TDD of 10^6 cm^{-2} [28]. At this TDD, the values of τ_n were 1.494 and 3.171 ns in the p-GaAs and the p-InGaP base, respectively, as calculated in Fig. 2.

We first varied the thickness of p-InGaP base from 1.1 to 0.3 μm in a 1J InGaP cell configuration. This is represented by the blue curve in Fig. 6(a). Then, in the 2J cell configuration, the thickness of p-InGaP base was again varied over the same range with the GaAs base thickness set to 1 μm (pink curve), as shown in Fig. 6(a). The same procedure was repeated for the GaAs base thickness of 2 (black curve) and 3 μm (red curve). The InGaP cell structure was the same in both the 1J InGaP and the 2J InGaP/GaAs cell configurations. It can be seen that thinning the base thickness in the 1J InGaP cell lowered the $J_{\rm sc}$ due to reduction in the absorption depth for the photons to be absorbed in the p-InGaP base. Interestingly, thinning the InGaP base thickness in the 2J cell configuration allowed more photons through to the bottom GaAs subcell, resulting in an increase of $J_{\rm sc}$ from the GaAs subcell at the cost of reduction in

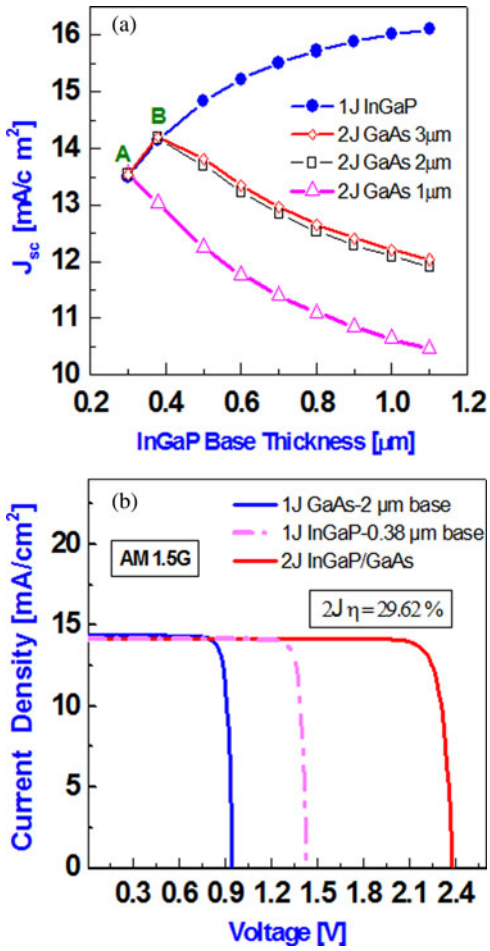

Fig. 6. (a) Short-circuit current density as a function of variation in the base thickness of the InGaP subcell to realize current matching. (b) Current-matched J–V characteristic of the 2J InGaP/GaAs cell on Si at AM 1.5G corresponding to the current-matched point B in Fig. 5(a).

$J_{\rm sc}$ from the InGaP subcell. This resulted in the overall increase in $J_{\rm sc}$ of 2J cell as the bottom GaAs subcell limited the $J_{\rm sc}$ in the 2J cell configuration. Furthermore, as the top cell base was being thinned, increasing the base thickness of the bottom GaAs subcell allowed for additional photons through to the GaAs subcell. This led to further improvement in the overall $J_{\rm sc}$ of the 2J cell. However, further increment in the GaAs base thickness beyond 2 μm did not result in significant improvement of $J_{\rm sc}$. This was likely due to insignificant photocurrent contribution from the GaAs subcell beyond a base thickness of 2 μm.

Utilizing the method discussed previously, the current-matching condition was realized at point A ($J_{\rm sc}$ = 13.5 mA/cm^2) and B ($J_{\rm sc}$ = 14.18 mA/cm^2), as shown in Fig. 6(a). The J–V characteristics of the 2J cell and the individual subcells corresponding to the point B were plotted in Fig. 6(b). At point B, the 2J cell exhibited a conversion efficiency of 29.62% with a 2-μm and a 0.38-μm-thick GaAs and InGaP base, respectively. The cell parameters extracted after achieving the current-matching condition between the two subcells at a TDD of 10^6 cm^{-2} were summarized in Table III. These results illustrate that even at a TDD of 10^6 cm^{-2}, an

TABLE III
2J InGaP/GaAs CELL PARAMETERS AT AM 1.5G ILLUMINATION

2J cell (InGaP/GaAs base thickness in μm)	V_{oc} (V)	J_{sc} (mA/cm^2)	FF (%)	Efficiency (%)
Non-optimized (0.9/2.5)	2.35	12.41	89.73	26.22
Current-matched (0.38/2)	2.37	14.18	88.22	29.62

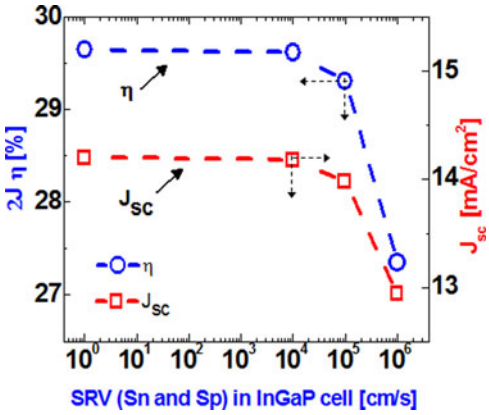

Fig. 7. 2J InGaP/GaAs cell η and J_{sc} as a function of SRV in the top InGaP subcell.

efficiency of greater than 29% can be realized for a metamorphic 2J InGaP/GaAs solar cell on Si by carefully engineering the cell design. To further verify the results from this simulation study, experimental work is underway.

D. Impact of Surface Recombination on 2J InGaP/GaAs Cell

Interface recombination could be a major factor that limits the performance of a tandem cell. Recombination at top cell interfaces was found to have the most detrimental impact [20]. In our design, the thickness of the top InGaP subcell was significantly reduced; hence, it was important to analyze the impact of SRV on the overall 2J cell performance. Fig. 7 shows the impact of SRV at top InGaP subcell interfaces on the 2J cell η and J_{sc}. Initially, all the SRVs were set to 10^0 cm/s at all the interfaces in the GaAs and the InGaP subcells. Thereafter, the SRV was set to 10^6 cm/s in the GaAs subcell, while the SRV in the InGaP subcell was varied. It can be seen that the SRV, when below 10^4 cm/s in the InGaP subcell, had negligible impact on the efficiency of the 2J cell. However, the efficiency dropped to 27.35% at an SRV of 10^6 cm/s due to degradation in J_{sc}. Thus, it is important to restrict the SRV below 10^4 cm/s in the InGaP subcell to achieve high-efficiency 2J InGaP/GaAs cell on Si.

IV. CONCLUSION

We have investigated the impact of TDD on the performance of 1J n$^+$/p GaAs and 2J n$^+$/p InGaP/GaAs cells on Si at AM 1.5G spectrum. The analysis indicates that in a 1J GaAs cell on Si with a 2.5-μm-thick GaAs base, an efficiency of greater than 23% can be realized at a TDD of 10^6 cm^{-2}. For both 1J and 2J cell configurations, the onset of degradation in V_{oc} was found to occur at a lower TDD than in J_{sc}, indicating that V_{oc} was more sensitive to TDD.

The 2J InGaP/GaAs cell at a TDD of 10^6 cm^{-2} exhibited an efficiency of 26.22% with a 2.5- and 0.9-μm-thick GaAs and InGaP base, respectively. The design of the 2J InGaP/GaAs cell on Si was optimized at a TDD of 10^6 cm^{-2} to achieve current matching between the two subcells. By thinning the top InGaP cell from 0.9 to 0.38 μm, the 2J cell efficiency increased to 29.62% from 26.22%. In addition, at the interfaces in the top InGaP subcell, the SRVs below 10^4 cm/s had negligible impact on the 2J cell performance. Thus, even in a lattice-mismatched 2J InGaP/GaAs cell on Si with TDD of 10^6 cm^{-2}, a theoretical conversion efficiency of greater than 29% at AM1.5G is achievable by tailoring the device design. Once experimentally realized, the III–V cell technology on Si would offer a new paradigm for the advancement of low-cost III–V solar cells and foster innovative avenues for both space and terrestrial applications.

REFERENCES

[1] J. F. Geisz, S. Kurtz, M. W. Wanlass, J. S. Ward, A. Duda, D. J. Friedman, J. M. Olson, W. E. McMahon, T. E. Moriarty, and J. T. Kiehl, "High-efficiency GaInP/GaAs/InGaAs triple-junction solar cells grown inverted with a metamorphic bottom junction," *Appl. Phys. Lett.*, vol. 91, pp. 023502-1–023502-3, Jul. 2007.

[2] W. Guter, J. Schone, S. P. Phillips, M. Steiner, G. Siefer, A. Wekkeli, E. Welser, E. Oliva, A. W. Bett, and F. Dimroth, "Current-matched triple-junction solar cell reaching 41.1% conversion efficiency under concentrated sunlight," *Appl. Phys. Lett.*, vol. 94, pp. 223504-1–223504-3, Jun. 2009.

[3] R. R. King, D. C. Law, K. M. Edmondson, C. M. Fetzer, G. S. Kinsey, H. Yoon, R. A. Sherif, and N. H. Karam, "40% efficient metamorphic GaInP/GaInAs/Ge multijunction solar cells," *Appl. Phys. Lett.*, vol. 90, pp. 183516-1–183516-3, Apr. 2007.

[4] S. Wojtczuk, P. Chiu, X. Zhang, D. Derkacs, C. Harris, D. Pulver, and M. Timmons, "InGaP/GaAs/InGaAs 41% concentrator cells using bifacial epigrowth," in *Proc. 35th IEEE Photovoltaic Spec. Conf.*, Jun. 2010, pp. 001259–001264.

[5] M. A. Green, K. Emery, Y. Hishikawa, W. Warta, and E. D. Dunlop, "Solar cell efficiency tables (ver. 39)," *Prog. Photovoltaics: Res. Appl.*, vol. 20, pp. 12–20, 2012.

[6] R. Tatavarti, A. Wibowo, G. Martin, F. Tuminello, C. Youtsey, G. Hillier, N. Pan, M. W. Wanlass, and M. Romero, "InGaP/GaAs/InGaAs inverted metamorphic (IMM) solar cells on 4″ epitaxial lifted off (ELO) wafers," in *Proc. 35th IEEE Photovoltaic Spec. Conf.*, Jun. 2010, pp. 002125–002128.

[7] G. J. Bauhuis, P. Mulder, E. J. Haverkamp, J. J. Schermer, E. Bongers, G. Oomen, W. Kostler, and G. Strobl, "Wafer reuse for repeated growth of III–V solar cells," *Prog. Photovoltaics: Res. Appl.*, vol. 18, pp. 155–159, 2010.

[8] R. K. Ahrenkiel, M. M. Al-Jassim, D. J. Dunlavy, K. M. Jones, S. M. Vernon, S. P. Tobin, and V. E. Haven, "Minority-carrier lifetime of GaAs on silicon," *J. Electrochem. Soc.*, vol. 137, pp. 996–1000, 1990.

[9] J. A. Carlin, S. A. Ringel, A. Fitzgerald, and M. Bulsara, "High-lifetime GaAs on Si using GeSi buffers and its potential for space photovoltaics," *Sol. Energy Mater. Sol. Cells*, vol. 66, pp. 621–630, Feb. 2001.

[10] S. M. Vernon, S. P. Tobin, M. M. Al-Jassim, R. K. Ahrenkiel, K. M. Jones, and B. M. Keyes, "Experimental study of solar cell performance versus dislocation density," in *Proc. 21st IEEE Photovoltaic Spec. Conf.*, May 1990, pp. 211–216.

[11] M. Yamaguchi, A. Yamamoto, and Y. Itoh, "Effect of dislocations on the efficiency of thin-film GaAs solar-cells on Si substrates," *J. Appl. Phys.*, vol. 59, pp. 1751–1753, Mar. 1986.

[12] M. Yamaguchi, C. Amano, and Y. Itoh, "Numerical-analysis for high-efficiency GaAs solar-cells fabricated on Si substrate," *J. Appl. Phys.*, vol. 66, pp. 915–919, Jul. 1989.

[13] C. L. Andre, D. M. Wilt, A. J. Pitera, M. L. Lee, E. A. Fitzgerald, and S. A. Ringel, "Impact of dislocation densities on n(+)/p and p(+)/n junction GaAs diodes and solar cells on SiGe virtual substrates," *J. Appl. Phys.*, vol. 98, pp. 014502-1–014502-5, Jul. 2005.
[14] J. C. Zolper and A. M. Barnett, "The effect of dislocations on the open-circuit voltage of gallium-arsenide solar-cells," *IEEE Trans. Electron Devices*, vol. 37, no. 2, pp. 478–484, Feb. 1990.
[15] G. F. Brown, J. W. Ager, W. Walukiewicz, and J. Wu, "Finite element simulations of compositionally graded InGaN solar cells," *Sol. Energy Mater. Sol. Cells*, vol. 94, pp. 478–483, Mar. 2010.
[16] H. Zhang, N. Chen, Y. Wang, X. Zhang, Z. Yin, H. Shi, Y. Wang, T. Huang, Y. Bai, and Z. Fu, "Evaluating the effect of dislocation on the photovoltaic performance of metamorphic tandem solar cells," *Sci. China Technol. Sci.*, vol. 53, pp. 2569–2574, 2010.
[17] M. L. Lovejoy, M. R. Melloch, and M. S. Lundstrom, "Minority hole mobility in GaAs," in *Properties of Gallium Arsenide*. (Data Review Series no. 16), M. R. Brozel and G. E. Stillman, Eds., London, U.K.: INSPEC, 1996, pp. 123–130.
[18] R. K. Ahrenkiel and M. S. Lundstrom, "Minority carrier transport in III-V semiconductors," in *Minority Carrier in III-V Semiconductors: Physics and Applications* (Semiconductors and Semimetals), vol. 39, R. K. Willardson, A. C. Beer, and E. R. Weber, Eds., New York: Academic, 1993, pp. 193–258.
[19] C. L. Andre, J. J. Boeckl, D. M. Wilt, A. J. Pitera, M. L. Lee, E. A. Fitzgerald, B. M. Keyes, and S. A. Ringel, "Impact of dislocations on minority carrier electron and hole lifetimes in GaAs grown on metamorphic SiGe substrates," *Appl. Phys. Lett.*, vol. 84, pp. 3447–3449, May 2004.
[20] M. Y. Ghannam, J. Poortmans, J. F. Nijs, and R. P. Mertens, "Theoretical study of the impact of bulk and interface recombination on the performance of GaInP/GaAs/Ge triple junction tandem solar cells," in *Proc. 3rd World Conf Photovoltaic Energy Convers.*, May 2003, pp. 666–669.
[21] T. Takamoto, M. Yamaguchi, S. J. Taylor, M.-J. Yang, E. Ikeda, and H. Kurita, "Radiation resistance of high-efficiency InGaP GaAs tandem solar cells," *Sol. Energy Mater. Sol. Cells*, vol. 58, pp. 265–276, Jul. 1999.
[22] T. Takamoto, E. Ikeda, H. Kurita, and M. Ohmori, "Structural optimization for single junction InGaP solar cell," *Sol. Energy Mater. Sol. Cells*, vol. 35, pp. 25–31, Sep. 1994.
[23] "APSYS, Advanced Physical Models of Semiconductor Devices," Crosslight Software Inc., Burnaby, BC, Canada.
[24] M. Yamaguchi and C. Amano, "Efficiency calculations of thin-film GaAs solar-cells on Si substrates," *J. Appl. Phys.*, vol. 58, pp. 3601–3606, 1985.
[25] M.-J. Yang, M. Yamaguchi, T. Takamoto, E. Ikeda, H. Kurita, and M. Ohmori, "Photoluminescence analysis of InGaP top cells for high-efficiency multi-junction solar cells," *Sol. Energy Mater. Sol. Cells*, vol. 45, pp. 331–339, Feb. 1997.
[26] T. Takamoto, E. Ikeda, H. Kurita, and M. Ohmori, "Over 30% efficient InGaP/GaAs tandem solar cells," *Appl. Phys. Lett.*, vol. 70, pp. 381–383, Jan. 1997.
[27] C. Algora, I. Rey-Stolle, I. Garcia, B. Galiana, M. Baudrit, and J. R. Gonzalez, "Lattice-matched III–V dual-junction solar cells for concentrations around 1000 suns," *J. Sol Energy Eng.*, vol. 129, pp. 257–346, 2007.
[28] Y. Takano, M. Hisaka, N. Fujii, K. Suzuki, K. Kuwahara, and S. Fuke, "Reduction of threading dislocations by InGaAs interlayer in GaAs layers grown on Si substrates," *Appl. Phys. Lett.*, vol. 73, pp. 2917–2919, 1998.
[29] S. R. Kurtz, P. Faine, and J. M. Olson, "Modeling of two-junction, series-connected tandems solar cells using top-cell thickness as an adjustable parameter," *J. Appl. Phys.*, vol. 68, pp. 1890–1895, 1990.

Nikhil Jain (S'12) received the B.S. degree (Hons.) in electrical and computer engineering from the University of Illinois at Urbana-Champaign in 2010. He is currently working toward the M.S./Ph.D. degree with the Bradley Department of Electrical Engineering, Virginia Tech, Blacksburg.

His current research focus is on the heterogeneous integration of III–V multijunction solar cells on Si. His research interests include design and epitaxial growth of compound semiconductor materials and devices for sustainable energy and low-power transistor applications.

Mr. Jain received the John Bardeen Award and the International Student and Scholar Services Undergraduate Scholarship while he was an undergraduate student with the University of Illinois. He was nominated for the Best Student Poster Award at the 2012 Photovoltaic Specialists Conference, Austin, TX.

Mantu K. Hudait (M'08–SM'08) received the M.S. degree in materials science and engineering from the Indian Institute of Technology Kharagpur, India, with specialization in semiconductor and allied materials, and the Ph.D. degree in materials science and engineering from the Indian Institute of Science, Bangalore, India, in 1999. His Ph.D. dissertation was on III–V solar cells on Ge and GaAs using metal–organic vapor-phase epitaxy.

From 2000 to 2005, he was a Postdoctoral Researcher with The Ohio State University, Columbus, where he was involved in research on the mixed cation and mixed anion metamorphic graded buffer, carrier transport in mixed anion system, low bandgap thermophotovoltaics, and heterogeneous integration of III–V solar cells on Si using SiGe buffer. From 2005 to 2009, he was a Senior Engineer with the Advanced Transistor and Nanotechnology Group, Intel Corporation. His breakthrough research in low-power transistors on Si at Intel Corporation was press released in 2007 and 2009. In 2009, he joined the Bradley Department of Electrical and Computer Engineering, Virginia Tech, Blacksburg, as an Associate Professor. He has more than 115 technical publications and refereed conference proceedings and holds 34 patents. His current research at Virginia Tech focuses on heterogeneous integration of compound semiconductors and Ge on Si for ultralow power logic and photovoltaics. His research interests include III–V compound semiconductor epitaxy, defect engineering in nanoscale, metamorphic buffers, devices for sustainable energy-related applications, including thermophotovoltaics and III–V and Ge quantum well and tunnel field-effect transistors.

Dr. Hudait has received two Divisional Recognition Awards from Intel Corporation. He is a member of the American Vacuum Society and the American Society for Engineering Education.